Using the fractional interaction law to model the impact dynamics of multiparticle collisions in arbitrary form

Jacek S. Leszczynski*
Czestochowa University of Technology, Institute of Mathematics and Computer Science, ul. Dabrowskiego 73, 42-200 Czestochowa, Poland
(Received 7 April 2004; published 29 November 2004)

Using the molecular dynamics method, we examine a discrete deterministic model for the motion of spherical particles in three-dimensional space. The model takes into account multiparticle collisions in arbitrary forms. Using fractional calculus we proposed an expression for the repulsive force, which is the so-called fractional interaction law. We then illustrate and discuss how to control (correlate) the energy dissipation and the collisional time for an individual particle within multiparticle collisions. We included in the multiparticle collisions the friction mechanism needed for the transition from coupled torsion-sliding friction through rolling friction to static friction. Analyzing simple simulations we found that binary collisions dominate in the strong repulsive state. However, weak repulsion is observed to be much stronger within multiparticle collisions. The presented numerical results can be used to realistically model the impact dynamics of an individual particle in a group of colliding particles.

DOI: 10.1103/PhysRevE.70.051315 PACS number(s): 45.05.+x, 45.70.−n, 45.50.Tn, 83.10.Pp

I. INTRODUCTION

The nature of particle flows offers the physics and engineering communities an opportunity to analyse the interesting behaviour of granular materials. From a phenomenological point of view such a flow, being halfway between a solid and a liquid state, is not well understood because the basic physics is extremely complex. In a local state, the simplest form of the granular dynamics is as follows: during particle motions the particles move individually and exchange their momenta and energies through particle collisions. Therefore the collision process plays a dominant role in the development of theoretical studies and also in the performance of simulations. For an understanding of the collision process we need to consider a simple situation, focusing on what happens when two particles collide. In other words, we need to be able to distinguish the following basic phenomena: static contact [1], cohesion [2,3], attrition [4], erosion [5], and fragmentation [6]. These phenomena may occur simultaneously or respectively when an individual particle impacts with another. After impact, separation [7] or clusterization [8] of the two particles occurs. In addition, the particles may gain or loss mass.

Here we will focus on the dynamics of the collision process, which may be decomposed into impact and contact processes. However, as the contact process is formed, we can also notice rebound [7] or static contact [1], or permanent contact, called cohesion [2]. These processes exist simultaneously when we analyze the dynamics of colliding particles. With regard to the granular dynamics involving many particles in motion, we can observe multiparticle collisions [9], especially when particle concentration is very dense, because collisional times between several binary particle contacts are higher in comparison to their separation times. Multiparticle collisions occur when an individual particle collides with neighboring particles, so that those contacts have direct a influence on each other. Only an infinitesimally short collisional time is required for binary collisions [7].

In all the considered cases the collision process between the two particles is characterized through the collisional time, which is dependent on the impact energy, and the physical properties of the contacting surfaces. Moreover, dissipation of energy occurs between the colliding particles after impact. Therefore the simulations of such dynamics are limited by assumptions concerning the collision process. One of the major aspects which needs to be taken into account in the simulations is how to control (correlate) the collisional time and the energy dissipation associated with an individual particle during the dynamics of multiparticle collisions.

Generally two different ways of modeling the dynamics of a granular material exist. The continuum approach [10] is based on binary collisions of smooth spherical particles. Unfortunately, the introduction of real quantities such as the distribution of particle dimensions, particle shapes, their surface wetness and roughness, etc., greatly limits the application of continuum models. Balzer *et al.* [11] inform us that kinetic theory is useful for modeling gas-solid flow applications in industry: where the geometry involved is complex (many different inlets or/and outlets). However, kinetic theory cannot reflect the real dynamics involved in multiparticle collisions because the collisional time is defined only for binary collisions.

The discrete deterministic approach more realistically reflects the collision process. Note that multiparticle collisions in the discrete approach are decomposed into several binary collisions. One may distinguish two general methods in this approach. The molecular dynamics method [12] takes into account an expression for the repulsive force acting between a pair of contacting particles. In this method particles virtually overlap when a contact occurs. The overlap reflects the quantitative deformations of particle surfaces because the

*Electronic address: jale@imi.pcz.pl

modeling of realistic deformations would be much too complicated. The interaction laws [13–15] in the molecular dynamics method define basic models of the repulsive force for two colliding particles. They are valid for particle collisions which are independent of one another. The next method, called the event driven method [16], assumes instantaneous changes in the direction and value of particle velocities, according to conservation equations, each time a binary contact occurs. As shown in [17] the basic difference between the event driven and molecular dynamics methods is the collisional time between a pair of particles. In the event driven method this time is ideally zero. Note that this situation is quite different for the molecular dynamics method, where the contact time is greater than zero and is dependent on parameters describing the structure of two contacting surfaces, and is, of course, dependent on the impact energy. The repulsive force models in the molecular dynamics method underestimate the energy dissipation in multiparticle collisions [18,19] (This is the so-called "detachment effect"), while in the event driven method an inelastic collapse [20] occurs.

In this paper we will focus on the molecular dynamics method because this gives us a chance to correlate the collisional time and the energy dissipation during multiparticle collisions. We shall introduce a different mathematical description of this method taking into account the division of the collision process into an impact phase, a contact phase and another phase occurring after the contact phase. We assume that the impact phase and the phase formed after the contact phase are infinitesimally short in time. Consequently, we will analyze the well-known interaction laws of the repulsive force in the contact phase in order to examine several difficulties within the collisions. On the base of preliminary results [21] we shall introduce another form of the repulsive force defined under fractional calculus [22,23]. We will also demonstrate the basic properties of this force and focus on what happens with the collisional time and the energy dissipation in multiparticle collisions. This analysis is necessary in computational simulations of the cluster dynamics because one may notice nonpermanent contact and/or cohesion phenomena between several pairs of colliding particles within the cluster.

II. THE DISCRETE MODEL OF MOTION FOR AN INDIVIDUAL PARTICLE

Let us turn our attention to a set of spherical particles moving under extortion. The spherical shape of the particle makes only the mathematical description easier and does not make the model in any way poorer. The reader may find in [24] more information concerning the molecular dynamics technique adapted to particle shapes in arbitrary form. The particles are numbered by the discrete index $i=1,\ldots,np$, where np is the total number of considered particles. We describe an individual particle through its radius r_i (or diameter d_i), mass m_i, inertia moment $\mathcal{J}_i$, position $\mathbf{x}_i$ of the mass center, linear speed $\dot{\mathbf{x}}_i$ and angular velocity $\boldsymbol{\omega}_i$. With regard to the collision of two individual particles we also introduce the function $j(i)$ [$j(i)\neq i$ by assumption] of a particle i in order to find the particle index of a particle in a set of particles np. Several papers [25–27] present different algorithms that detect particle collisions, being dependent on their shapes, and consequently that to find the function $j(i)$. To simplify our notation we will use j instead of $j(i)$. For a binary collision we neglect phenomena which cause a change in the mass of an individual particle. Thus, in our discrete model, we do not take into account fragmentation, attrition and erosion which eventually take place during the collision process. These phenomena will be the subject of future investigations.

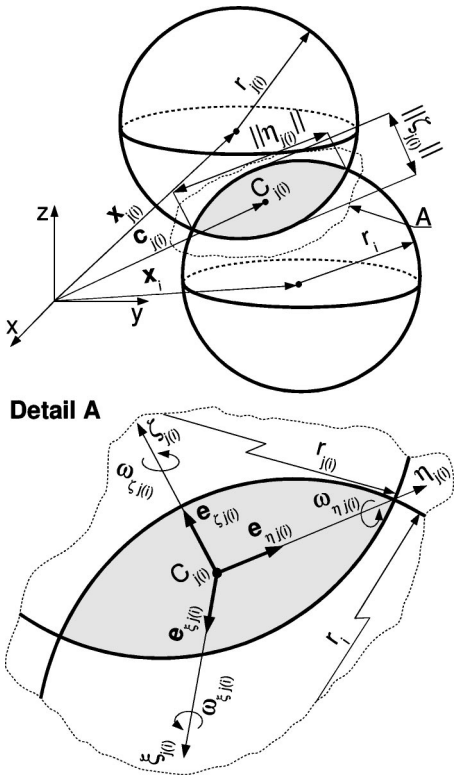

FIG. 1. Scheme illustrates particle collisions with useful notations.

However, after the contact, which is the second phase of the collision process, rebound, nonpermanent contact (static contact) or cohesion can arise simultaneously. In this paper, we will try to model the above phenomena by introducing a different mathematical description and a different form of the repulsive force into the molecular dynamics method.

A. Mapping local coordinates onto global ones and defining the overlap

Starting from the description shown in Fig. 1, let us introduce several definitions before formulating the motion equations. First, we assign local coordinates as (ξ,η,ζ) and global ones as (x,y,z). When we consider a contact, which eventually takes place between two particles, then the normal unit vector $\mathbf{e}_{\zeta j}$ that connects the particles' centers of mass reads

$$\mathbf{e}_{\zeta j}=\frac{\mathbf{x}_j-\mathbf{x}_i}{\|\mathbf{x}_j-\mathbf{x}_i\|}=[e^x_{\zeta j},e^y_{\zeta j},e^z_{\zeta j}], \tag{1}$$

where $\|\cdot\|$ represents a norm calculated from the relative coordinate $\mathbf{x}_j-\mathbf{x}_i$. Tangential unit vectors which operate on a

tangent plane (rotated by $\pi/2$ to the normal) become

$$\mathbf{e}_{\eta j} = [e^{y}_{\zeta j}, -e^{x}_{\zeta j}, 0]\frac{\|\mathbf{x}_j - \mathbf{x}_i\|}{\|\mathbf{x}_j - \mathbf{x}_i\|_{x,y}}, \tag{2}$$

$$\mathbf{e}_{\xi j} = \mathbf{e}_{\eta j} \times \mathbf{e}_{\zeta j}, \tag{3}$$

where $\|\cdot\|_{x,y}$ represents the norm which is calculated only in the tangent plane. When a particle hits a wall we redefine unit vectors (1)–(3) putting $\mathbf{xb}_j$ instead of $\mathbf{x}_j$, where $\mathbf{xb}_j$ is a point whose coordinates issue from the line that crosses the particle's center of mass and is perpendicular to the wall. The general form of the base vectors is presented as follows:

$$\mathbf{e}_j = \begin{bmatrix} \mathbf{e}_{\xi j} \\ \mathbf{e}_{\eta j} \\ \mathbf{e}_{\zeta j} \end{bmatrix}. \tag{4}$$

Figure 1 presents the "virtual overlap" $\|\boldsymbol{\zeta}_j\|$ of two particles experiencing a contact. With regard to [28] we define the overlap as

$$\|\boldsymbol{\zeta}_j\| = r_j + r_i - \|\mathbf{x}_j - \mathbf{x}_i\|, \tag{5}$$

which is associated with the particles having spherical forms. Note that only positive values of formula (5) indicate a contact while negative ones confirm that the considered particles are in separation, i.e., they move individually. As presented in previous section and in Fig. 1, the overlap reflects the penetration depth of the particles in the direction which connects the particles' centers of mass, in the direction from i to j. We also introduce the penetration width of the particles, defined as the direction perpendicular to the previous one. Thus we have

$$\|\boldsymbol{\eta}_j\| = \|\boldsymbol{\xi}_j\| = 2\sqrt{r_i^2 - \left(r_i + \frac{1}{2}\|\boldsymbol{\zeta}_j\|\frac{2r_j - \|\boldsymbol{\zeta}_j\|}{\|\boldsymbol{\zeta}_j\| - (r_i + r_j)}\right)^2} \tag{6}$$

valid for $\|\boldsymbol{\zeta}_j\| \geqslant 0$. Let $\mathbf{c}_j$ be a vector which defines a point C_j of the application of the repulsive force, and which is taken as the mass center of the overlapping region (5) as shown in Fig. 1. Taking into consideration the fact that the particles have only spherical forms and collide when their overlap (5) is positive we obtain

$$\mathbf{c}_j = \mathbf{x}_i + \left(r_i - \frac{\|\boldsymbol{\zeta}_j\|(r_j - \|\boldsymbol{\zeta}_j\|)}{r_i + r_j - \|\boldsymbol{\zeta}_j\|}\right)\mathbf{e}_{\xi j}. \tag{7}$$

Thus, at the beginning of a collision we have

$$\mathbf{c}_j = \frac{r_i\mathbf{x}_j + r_j\mathbf{x}_i}{r_j + r_i}, \tag{8}$$

and one can find a time t_j^b where the overlap (5) is zero. Above the notation allows us to analyze multiparticle collisions where an individual particle i collides with neighboring particles j. Therefore many overlaps (5) indexed j on the particle i may occur. This allows us to formulate the motion equations in the right form.

Next we introduce the relative velocity of a particle i and a particle j at point C_j as

$$\tilde{\mathbf{u}}_j = \tilde{\mathbf{u}}_j^{lin} - \tilde{\mathbf{u}}_j^{rot} = \dot{\mathbf{x}}_i - \dot{\mathbf{x}}_j + \boldsymbol{\omega}_i \times \tilde{\mathbf{s}}_j - \boldsymbol{\omega}_j \times \tilde{\tilde{\mathbf{s}}}_j, \tag{9}$$

where $\tilde{\mathbf{u}}_j^{lin}$ and $\tilde{\mathbf{u}}_j^{rot}$ are linear and rotational relative velocities and $\tilde{\mathbf{s}}_i$, $\tilde{\tilde{\mathbf{s}}}_j$ are branch vectors connecting the mass centers of particles i and j with the point C_j of application of the repulsive force. Note that the above values are defined for the global system of coordinates (x,y,z). To change this to the local system of coordinates we need to use the scalar product of the base vectors (4) and the vector of the relative velocity. Calculating the branch vectors we obtain the following dependencies in the local system (ξ, η, ζ) as

$$\tilde{\mathbf{s}}_j' = [0, 0, \|\tilde{\boldsymbol{\zeta}}_j\|], \quad \tilde{\tilde{\mathbf{s}}}_j' = [0, 0, -\|\tilde{\tilde{\boldsymbol{\zeta}}}_j\|], \tag{10}$$

where

$$\|\tilde{\boldsymbol{\zeta}}_j\| = \|\mathbf{c}_j - \mathbf{x}_i\| = r_i - \|\boldsymbol{\zeta}_j\|\frac{\frac{1}{2}\|\boldsymbol{\zeta}_j\| - r_j}{\|\boldsymbol{\zeta}_j\| - (r_i + r_j)}, \tag{11}$$

$$\|\tilde{\tilde{\boldsymbol{\zeta}}}_j\| = \|\mathbf{c}_j - \mathbf{x}_j\| = r_j - \|\boldsymbol{\zeta}_j\|\frac{\frac{1}{2}\|\boldsymbol{\zeta}_j\| - r_i}{\|\boldsymbol{\zeta}_j\| - (r_i + r_j)}. \tag{12}$$

In the global system of coordinates the branch vectors become

$$\tilde{\mathbf{s}}_j = \mathbf{e} \cdot \tilde{\mathbf{s}}_j'^{T}, \quad \tilde{\tilde{\mathbf{s}}}_j = \mathbf{e} \cdot \tilde{\tilde{\mathbf{s}}}_j'^{T}. \tag{13}$$

Using Eqs. (4) and (9) we translate the linear and rotational relative velocities in the global system of coordinates to the local one:

$$\tilde{\mathbf{u}}_j'^{\,lin} = \mathbf{e} \cdot \tilde{\mathbf{u}}_j^{lin}, \; \tilde{\mathbf{u}}_j'^{\,rot} = \mathbf{e} \cdot \tilde{\mathbf{u}}_j^{rot}, \tag{14}$$

where $\tilde{u}_{\xi j}^{lin}$, $\tilde{u}_{\xi j}^{rot}$ are the relative velocities operating in the normal direction to the contacting surfaces as shown in Fig. 1 and

$$\tilde{\mathbf{u}}_{tj}'^{\,lin} = [\tilde{u}_{\xi j}^{lin}, \; \tilde{u}_{\eta j}^{lin}], \; \tilde{\mathbf{u}}_{tj}'^{\,rot} = [\tilde{u}_{\xi j}^{rot}, \; \tilde{u}_{\eta j}^{rot}] \tag{15}$$

denote vectors of the relative velocities acting in the tangential direction (rotated by $\pi/2$ to the normal). Additionally we use the same translation as presented by expression (14) for calculations $\omega_i' = \mathbf{e} \cdot \omega_i$, $\omega_j' = \mathbf{e} \cdot \omega_j$ in order to obtain the angular velocities for particles i and j in the local system of coordinates (ξ, η, ζ).

If a collision between a particle and a wall takes place, the overlap (5) is defined as

$$\|\boldsymbol{\zeta}_j^b\| = r_i - \|\mathbf{xb}_j - \mathbf{x}_i\|, \tag{16}$$

and we also have

$$\|\boldsymbol{\eta}_j^b\| = 2\sqrt{\|\boldsymbol{\zeta}_j^b\|(2r_i - \|\boldsymbol{\zeta}_j^b\|)} \tag{17}$$

which is valid for $\|\zeta_j^b\| \geqslant 0$. In this case the point of application $\mathbf{c}_j^b$ is defined by the following formula:

$$\mathbf{c}_j^b = \mathbf{x}_i + \left(r_i - \frac{5}{8}\|\boldsymbol{\zeta}_j^b\|\right)\mathbf{e}_j^b, \tag{18}$$

where

$$\mathbf{e}_j^b = \frac{\mathbf{xb}_j - \mathbf{x}_i}{\|\mathbf{xb}_j - \mathbf{x}_i\|} \tag{19}$$

becomes a normal unit vector which is perpendicular to the wall. When a particle-wall collision begins we obtain $\mathbf{c}_j^b = \mathbf{x}_i + r_i \mathbf{e}_{\zeta j}^b$. Moreover, one can find the time t_j^{bb} when the overlap (16) is zero. Expressions (9)–(14), defined for a particle-particle collision, may be redefined for a particle-wall collision when $\dot{\mathbf{x}}_j$ and $\boldsymbol{\omega}_j$ are zeros, and the unit vectors are also redefined as explained in previously. For example a component of the branch vector (11) is redefined for a particle-wall collision and takes the following form:

$$\|\tilde{\boldsymbol{\zeta}}_j^b\| = r_i - \frac{5}{8}\|\boldsymbol{\zeta}_j^b\|. \tag{20}$$

We neglect here any additional expressions necessary to describe the particle-wall collision. This can be done this very easily in the same way as explained previously.

Summarizing our considerations, we have introduced the above mathematical description as it is necessary for the formulation of the motion equations and is also necessary for some forms of the repulsive force in both particle-particle and particle-wall collisions.

B. Motion equations

The molecular dynamics method requires a discrete deterministic approach in order to model the motion of an individual particle. As the particle may collide or lose contact with other particles, we need to add or reject some forms of the repulsive force and/or the attractive force in order to simulate the particle dynamics more realistically. In this paper, we will neglect the attractive force and concentrate only on the repulsive force. Against this background, let us describe the motion of an individual particle by the following two sets of equations

$$m_i \ddot{\mathbf{x}}_i = \sum_l \mathbf{F}_l,$$

$$\mathcal{J}_i \dot{\boldsymbol{\omega}}_i = \sum_l \mathbf{M}_l, \tag{21}$$

suitable for particle motion without any collision, and

$$m_i \ddot{\mathbf{x}}_i = \sum_{j,j\neq i} \mathbf{P}_j^{coll} + \sum_{j,j\neq i} \mathbf{P}_j^{b\ coll} + \sum_l \mathbf{F}_l,$$

$$\mathcal{J}_i \dot{\boldsymbol{\omega}}_i = \sum_{j,j\neq i} \tilde{\mathbf{M}}_j^{coll} + \sum_{j,j\neq i} \tilde{\mathbf{M}}_j^{b\ coll} + \sum_l \mathbf{M}_l, \tag{22}$$

which takes into account multiparticle collisions. The above sets of equations exist simultaneously over time and are dependent on the detection of a contact and the administration of the repulsive force-overlap path during the contact. In both Eqs. (21) and (22) $\mathbf{F}_l$ denotes a long range force which extorts the motion of a particle, $\mathbf{M}_l$ is a long range torque, $\mathbf{P}_j^{coll}$ is a collisional force composed of the repulsive and friction forces and acts between a pair of colliding particles, $\mathbf{P}_j^{b\ coll}$ is the collisional force operating on a particle-wall collision, $\tilde{\mathbf{M}}_j^{coll}$ and $\tilde{\mathbf{M}}_j^{b\ coll}$ are collisional torques operating on particle-particle and particle-wall collision.

We need to define some of the criteria necessary for handling the above sets of equations over the time of the calculations. It was shown in the previous subsection that at the beginning of a collision the overlap given by expression (5) or (16) is zero. Thus we have the impact phase. However, some of the criteria for determining when the collision ends are unclear. Correctly predicting the separation time of two colliding particles is crucial in the calculation. Most papers assume the particles separate at the time when the overlap returns to zero. As proved in [29], the repulsive force changes direction at the time when the overlap returns to zero. This is contrary to experimental evidence, also shown and compared with some models in [29], when the force does not change direction. An attractive force operating in opposite direction to the repulsive force has different origins and is not taken into account here.

At this crucial point of our considerations, we need to introduce some definitions in order to predict correctly the beginning time of a particle collision and the time when the collision ends. Let us consider the time of calculations $t \in \langle 0, T\rangle$ where T represents the total time in which the calculations are performed. We also define the time step Δt^{coll} in which we trace the system dynamics. It should be noted that $\Delta t^{coll} \ll t^{coll}$, where t^{coll} is a minimal value of the collisional time of two contacting particles. This assumption makes it possible to solve motion equations (22) in which collisional forces (torques) are included. In the next section we will present numerical criteria concerning the estimation of the collisional time. Following on from previous explanations we start with some conditions:

Definition 1. If, within a time interval $\langle t, t+\Delta t^{coll}\rangle$ the beginning of a collision between a pair of particles is detected, then the overlap (5) should fulfill the following conditions

$$\|\boldsymbol{\zeta}_j(t)\| \leqslant 0 \quad \text{and} \quad \|\boldsymbol{\zeta}_j(t+\boldsymbol{\Delta} t^{coll})\| \geqslant 0$$

$$\text{and therefore} \quad \|\boldsymbol{\zeta}_j(t_j^b)\| = 0, \tag{23}$$

and then time $t_j^b \in \langle t, t+\Delta t^{coll}\rangle$ is the time when the collision starts.

Definition 2. If the end of a collision is formed within a time interval $\langle t, t+\Delta t^{coll}\rangle$, then the overlap (5) and the normal component of the repulsive force $R_{\zeta j}$ should fulfill the following conditions

$$\|\boldsymbol{\zeta}_j(t)\| \geqslant 0 \quad \text{and} \quad \|\boldsymbol{\zeta}_j(t+\boldsymbol{\Delta} t^{coll})\| \leqslant 0$$

$$\text{and} \quad R_{\zeta j}(t) > 0 \quad \text{and} \quad R_{\zeta j}(t+\boldsymbol{\Delta} t^{coll}) > 0 \tag{24}$$

$$\text{and therefore} \quad \|\boldsymbol{\zeta}_j(t_j^e)\| = 0$$

or

$$\|\boldsymbol{\zeta}_j(t)\| > 0 \quad \text{and} \quad \|\boldsymbol{\zeta}_j(t+\boldsymbol{\Delta} t^{coll})\| > 0$$

$$\text{and} \quad R_{\zeta j}(t) \geqslant 0 \quad \text{and} \quad R_{\zeta j}(t+\boldsymbol{\Delta} t^{coll}) \leqslant 0 \tag{25}$$

$$\text{and therefore} \quad R_{\zeta j}(t_j^e) = 0,$$

and then time $t_j^e \in \langle t, t+\Delta t^{coll}\rangle$ is the time when the collision ends.

In formulas (24) and (25) $R_{\zeta\, j}$ represents a normal component of the repulsive force. We will introduce a definition of this force in the next subsection.

Definition 3. If, within a time interval $\langle t, t+\Delta t^{coll}\rangle$, the overlap and the normal component of the repulsive force $R_{\zeta j}$ behave as follows:

$$\|\boldsymbol{\zeta}_j(t)\| > 0 \quad \text{and} \quad \|\boldsymbol{\zeta}_j(t+\boldsymbol{\Delta} t^{coll})\| > 0$$

$$\text{and} \quad R_{\zeta j}(t+\boldsymbol{\Delta} t^{coll}) \to 0^+, \tag{26}$$

then time $t_j^e = \Delta t^{coll} + t$ is the time when the collision ends.

Definition 4. Within the binary collision for $t \in \langle t_j^b, t_j^e\rangle$ the linear and rotational components (14) of the relative velocity predict the following states:

variations in time of the overlap (5) for $\tilde{u}_{\zeta j}^{lin}(t) \neq 0$ [for $\tilde{u}_{\zeta j}^{lin}(t) > 0$ we have a compressed state but for $\tilde{u}_{\zeta j}^{lin}(t) < 0$ we obtain a decompressed state],

torsion for $\omega_{\zeta i}(t) - \omega_{\zeta j}(t) \neq 0$,

sliding for $\tilde{\mathbf{u}}_{tj}'^{\,lin}(t) \neq \tilde{\mathbf{u}}_{tj}'^{\,rot}(t)$ or rolling for $\tilde{\mathbf{u}}_{tj}'^{\,lin}(t) = \tilde{\mathbf{u}}_{tj}'^{\,rot}(t) \neq 0$.

Definition 5. When condition (24) is fulfilled then the component of the relative velocity in the normal direction $\tilde{u}_{\zeta j}(t_j^e) = -\tilde{u}_{\zeta j}(t_j^b)$ predicts the elastic rebound of particles.

Definition 6. When condition (25) is fulfilled then the values of the relative velocities (14) predict the particle behaviors after the collision as follows:

rebound with particle deformations for $\tilde{u}_{\zeta j}(t_j^e) < -\tilde{u}_{\zeta j}(t_j^b)$,

dynamic contact for $\tilde{u}_{\zeta j}(t_j^e) = 0$, in which eventually torsion $[\omega_{\zeta i}(t_j^e) - \omega_{\zeta j}(t_j^e) \neq 0]$ with sliding $[\tilde{\mathbf{u}}_{tj}'^{\,lin}(t_j^e) \neq \tilde{\mathbf{u}}_{tj}'^{\,rot}(t_j^e)]$ or with rolling $[\tilde{\mathbf{u}}_{tj}'^{\,lin}(t_j^e) = \tilde{\mathbf{u}}_{tj}'^{\,rot}(t_j^e) \neq 0]$ exists,

static contact for $\tilde{\mathbf{u}}_j'^{\,lin}(t_j^e) = \tilde{\mathbf{u}}_j'^{\,rot}(t_j^e) = 0$ and $\boldsymbol{\omega}_i(t_j^e) = \boldsymbol{\omega}_j(t_j^e) = 0$.

Definition 7. When condition (26) is fulfilled then the normal component $\tilde{u}_{\zeta j}^{lin}(t_j^e)$ of the relative velocity (14) predicts adhesion-induced plastic deformations of particles or breakage of particles depending on the hardness of the contacting surfaces.

On the basis of previous assumptions and definitions 1 and 2, we introduce the collisional time between a pair of contacting particles as $t_j^{coll} = t_j^e - t_j^b$. This time is determined by conditions (24) and (25) simultaneously. In other words, when the overlap changes sign faster than the repulsive force changes direction or vice versa then the collision is finished. If particles are still in contact, then the total contact time is significantly greater than the collisional time. If particles are separated, then the total contact time equals the collisional time. As presented in the first section, the collisional process is composed of the impact phase, the contact phase and the last phase formed after the contact phase. When the formulation of the first and the last phases is infinitesimally short in time then the collisional time is predicted by the contact phase. The contact phase is predicted by the repulsive force-overlap path. The adhesion or cohesion states extend the contact phase over time to infinity. In our approach adhesion and cohesion are eventually formed after the impact and they represent completely different phenomena which result from the collision process. Generally, when we model impact dynamics we need to consider the balance between the repulsive force, which is a direct reaction to the impact, and the attractive forces which are a result of, i.e., cohesion of particles. Therefore, our collisional time t_j^{coll} also becomes the time of relaxation in which the collision process is stopped and novel states are formed. Most papers neglect this fact and identify the total contact time, which may increase to infinity, as the collisional one.

Extending our considerations we notice that definition 5 is suitable for the elastic collisions of particles because there are no deformations in the contacting particles—the overlap tends to zero faster than the repulsive force changes direction. In definition 6 we observe the opposite situation—the repulsive force changes direction faster than the overlap tends to zero. In our approach the collision process is fully controlled by the repulsive force except for the situation presented by formula (26) in definition 3. On the basis of definition 7, which results from definition 3, we are able to explain that the local stresses associated with the deformations of contacting particles become sufficiently large so as to exceed the elastic limit of the materials and as a result plastic flow occurs [30] and the behavior of particle adhesion differs from that predicted by the elastic deformation theory [31]. Adhesion-induced plastic deformations of contacting materials are shown in some experiments [32]. Therefore we have two possible states resulting from the impact: particle clusterizations when the colliding materials are soft, and fragmentation of particles when the colliding materials are hard.

Summarizing this subsection—we formulated two general forms of the motion equations and discussed precisely how to handle them.

C. Collisional forces, collisional torques and the fractional interaction law

We introduce a mathematical description of the collisional forces and torques occurring in motion equations (22). We apply only a repulsive force in the normal direction to the contacting surfaces, completely neglecting any attractive forces. One can find some forms of attractive forces and their physical meanings in [3]. We introduce a system of friction forces and torques in a tangential plane. According to the friction mechanism, the tangential friction force is one of four types: torsion with sliding friction, sliding friction, rolling friction or static friction. Torsion friction occurs when colliding particles differ by their angular velocities in the normal direction $\omega_{\zeta i}$ and $\omega_{\zeta j}$. Torsion with sliding friction is for colliding particles which have different angular velocities in the normal direction and different linear velocities in the tangential plane. Sliding friction happens when slipping occurs in colliding particles. When the relative linear velocity of the particles in the tangent direction reduces to zero, sliding friction is replaced by rolling friction. If the external forces are sufficiently small, rolling friction reduces the velocity until particle motion stops and static friction occurs. Considering the impact dynamics, we implemented the fol-

lowing mechanism in general form: torsion with sliding friction can change to rolling friction, and rolling friction tends to static friction. More details concerning the modeling of torsion, sliding and rolling friction can be found in [33,34]. Here we show a description of the collisional force in global coordinates (x,y,z) as

$$\mathbf{P}_j^{coll} = \begin{cases} \mathbf{P}_j^{sta} & \text{for} \quad \|\tilde{\mathbf{u}}_{tj}'^{\,lin}\| = \|\tilde{\mathbf{u}}_{tj}'^{\,rot}\| = 0, \\ \mathbf{P}_j^{rol} & \text{for} \quad \|\tilde{\mathbf{u}}_{tj}'^{\,lin} - \tilde{\mathbf{u}}_{tj}'^{\,rot}\| = 0, \\ \mathbf{P}_j^{sli} & \text{for} \quad \|\tilde{\mathbf{u}}_{tj}'^{\,lin} - \tilde{\mathbf{u}}_{tj}'^{\,rot}\| > 0, \end{cases} \tag{27}$$

where $\mathbf{P}_j^{sta}$ is the force acting in a static friction state, $\mathbf{P}_j^{rol}$ is the force occurring in a rolling state and $\mathbf{P}_j^{sli}$ is the force coupling the torsion-sliding state. The emphasis in this paper is on the impact dynamics of static friction which is only implemented in a simple form. A more detailed model of the static friction state requires analysis of the tangential displacement and possibly the inclusion of time dependent effects. According to Fig. 1 we need to define the collisional force in the local system of coordinates (ξ,η,ζ). Using a matrix of the base vectors (4) we introduce transition from the local system to the global ones as

$$\mathbf{P}_j^{sli} = \mathbf{e}_j^T \cdot \mathbf{P}_j'^{\,sli}, \quad \mathbf{P}_j^{rol} = \mathbf{e}_j^T \cdot \mathbf{P}_j'^{\,rol}, \tag{28}$$

where $\mathbf{P}_j'^{\,sli}$, $\mathbf{P}_j'^{\,rol}$ are forces defined in the local system of coordinates as

$$\mathbf{P}_j'^{\,sli} = \begin{bmatrix} T_{\xi j}^{sli} \\ T_{\eta j}^{sli} \\ -R_{\zeta j} \end{bmatrix}, \quad \mathbf{P}_j'^{\,rol} = \begin{bmatrix} T_{\xi j}^{rol} \\ T_{\eta j}^{rol} \\ -R_{\zeta j} \end{bmatrix}. \tag{29}$$

In expression (29) $T_{\xi j}^{sli}$, $T_{\eta j}^{sli}$, $T_{\xi j}^{rol}$, $T_{\eta j}^{rol}$ represent components of the friction force in a plane (ξ,η) for torsion-sliding and rolling states, $R_{\zeta j}$ is a sum of the normal components of attractive and repulsive forces operating during a collision. As assumed in this paper, we neglect attractive forces and concentrate only on forms of the repulsive force. Some forms of the attractive forces can be found in [2,3] but the most well-known forms of the repulsive force are in [13–15].

On the basis of preliminary results [21] we now introduce a model of the repulsive force in general form called the fractional interaction law. Thus we have

$$R_{\zeta j} = \begin{cases} \max[0, c_j^{\alpha_j} k_j^{1-\alpha_j} {}_{t_j^b}\mathcal{D}_{t_j^e}^{\alpha_j}(\|\boldsymbol{\zeta}_j\|)] & \text{for} \quad \|\boldsymbol{\zeta}_j\| \geqslant 0, \\ 0 & \text{for} \quad \|\boldsymbol{\zeta}_j\| < 0, \end{cases} \tag{30}$$

where c_j, k_j are damping and spring coefficients with the same meaning as in the linear interaction law [13], $\|\boldsymbol{\zeta}_j\|$ represents the overlap defined by formula (5), t_j^b, t_j^e are start and stop times of a collision (not a total contact) predicted by several definitions in the previous subsection, α_j is the conversion degree of impact energy into viscoelasticity of the material and ${}_{t_j^b}\mathcal{D}_{t_j^e}^{\alpha_j}(\|\boldsymbol{\zeta}_j\|)$ represents the general form of the differential and integral operator of fractional order as explained in [21]. According to fractional calculus [22,23,35] we introduce the definition of this operator in the following form:

$${}_{t_j^b}\mathcal{D}_{t_j^e}^{\alpha_j}(\|\boldsymbol{\zeta}_j(t)\|) = \begin{cases} \displaystyle\sum_{l=0}^{n-1} \frac{(t-t_j^b)^{l-\alpha_j}}{\Gamma(l-\alpha_j+1)} \|\boldsymbol{\zeta}_j^{(l)}(t_j^b)\| + {}_{t_j^b}^{C}D_{t_{je}}^{\alpha_j}(\|\boldsymbol{\zeta}_j(t)\|) & \text{for } \alpha_j \geqslant 0, \\ {}_{t_j^b}I_{t_j^e}^{-\alpha_j}(\|\boldsymbol{\zeta}_j(t)\|) & \text{for } \alpha_j < 0, \end{cases} \tag{31}$$

where t denotes actual time of calculations $t \in \langle t_j^b, t_j^e \rangle$, the sum represents the initial conditions, ${}_{t_j^b}^{C}D_{t_j^e}^{\alpha_j}(\|\boldsymbol{\zeta}_j(t)\|)$ is the Caputo fractional derivative

$${}_{t_j^b}^{C}D_{t_j^e}^{\alpha_j}(\|\boldsymbol{\zeta}_j(t)\|) = \begin{cases} \dfrac{1}{\Gamma(n_j-\alpha_j)} \displaystyle\int_{t_j^b}^{t_j^e} \frac{\dfrac{d^{n_j}}{d\tau^{n_j}}\|\boldsymbol{\zeta}_j(\tau)\|}{(t_j^e-\tau)^{\alpha_j-n_j+1}} d\tau & \text{for } n_j - 1 < \alpha_j < n_j, \\ \dfrac{d^{n_j}}{d(t-t_j^e)^{n_j}}\|\boldsymbol{\zeta}_j(t)\| & \text{for } \alpha_j = n_j, \end{cases} \tag{32}$$

where $n_j = [\alpha_j] + 1$ and $[\cdot]$ denotes an integer part of a real number, and ${}_{t_j^b}I_{t_j^e}^{\beta_j}(\|\boldsymbol{\zeta}_j(t)\|)$ is the Riemann-Liouville fractional integral

$${}_{t_j^b}I_{t_j^e}^{\beta_j}(\|\boldsymbol{\zeta}_j(t)\|) = \begin{cases} \dfrac{1}{\Gamma(\beta_j)} \displaystyle\int_{t_j^b}^{t_j^e} \|\boldsymbol{\zeta}_j(\tau)\|(t_j^e-\tau)^{\beta_j-1} d\tau & \text{for } \beta_j \in \mathcal{R}^+, \\ \dfrac{1}{(\beta_j-1)!} \displaystyle\int_{t_j^b}^{t_j^e} \|\boldsymbol{\zeta}_j(\tau)\|(t_j^e-\tau)^{\beta_j-1} d\tau & \text{for } \beta_j \in \mathcal{N} \end{cases} \tag{33}$$

and $\beta_j = -\alpha_j$. Equation (30) represents the form of the repulsive force acting in the normal direction to the contacting surfaces.

Now we introduce additional definitions of forces operating in the tangent plane. Here we define the normal force as $\mathbf{N}'_j=[0,0,R_{\zeta j}]$. According to [33] we define the friction force which is coupled between torsion-sliding friction as

$$\mathbf{T}'^{\,sli}_j = -\mu(\|\tilde{\mathbf{u}}'^{\,lin}_{t\,j}\|)\mathcal{F}(\lambda_j)N_{\zeta\,j}\begin{bmatrix}\mathrm{sgn}(\tilde{u}^{lim}_{\xi j}-\tilde{u}^{rot}_{\xi j})\\ \mathrm{sgn}(\tilde{u}^{lim}_{\eta j}-\tilde{u}^{rot}_{\eta j})\\ 0\end{bmatrix}, \quad (34)$$

where the friction coefficient is

$$\mu(\|\tilde{\mathbf{u}}'^{\,lin}_{tj}\|) = \mu_d + (\mu_s-\mu_d)e^{-a\|\tilde{\mathbf{u}}'^{\,lin}_{tj}\|}, \quad (35)$$

where a is a numerical constant, μ_s and μ_d are static and dynamic coefficients of friction. Moreover in formula (34) the function $\mathcal{F}(\lambda_j)$ is defined according to [33] as

$$\mathcal{F}(\lambda_j)=\begin{cases}\dfrac{4}{3}\dfrac{(\lambda_j^2+1)E(\lambda_j)+(\lambda_j^2-1)K(\lambda_j)}{\pi\lambda_j} & \text{for } \lambda\leqslant 1,\\ \dfrac{4}{3}\dfrac{(\lambda_j^2+1)E\left(\dfrac{1}{\lambda_j}\right)-(\lambda_j^2-1)K\left(\dfrac{1}{\lambda_j}\right)}{\pi} & \text{for } \lambda>1,\end{cases} \quad (36)$$

where $K(\lambda_j)$ and $E(\lambda_j)$ are the complete elliptic integral functions of the first and the second kind, λ_j is the dimensionless quantity defined as

$$\lambda_j=\frac{\|\tilde{\mathbf{u}}'^{\,lin}_{tj}-\tilde{\mathbf{u}}'^{\,rot}_{tj}\|}{\frac{1}{2}\|\boldsymbol{\eta}_j\|\|\boldsymbol{\omega}_{\zeta i}-\boldsymbol{\omega}_{\zeta j}|}. \quad (37)$$

The limiting values of the function $\mathcal{F}(\lambda_j)$ are $\mathcal{F}(0)=0$ for torsion without sliding and $\lim_{\lambda_j\to\infty}\mathcal{F}(\lambda_j)=1$ for sliding without torsion.

According to [34] we define the rolling friction force as

$$\mathbf{T}'^{\,rol}_j=\frac{\frac{1}{\mathcal{J}_i}\widetilde{\mathbf{ss}}'_j\times\mathbf{N}_j\times\tilde{\mathbf{s}}'_j+\frac{1}{\mathcal{J}_j}\widetilde{\widetilde{\mathbf{ss}}}'_j\times\mathbf{N}_j\times\tilde{\tilde{\mathbf{s}}}'_j-\mathbf{A}_j}{\frac{1}{m_i}+\frac{1}{m_j}+\frac{(\|\tilde{\boldsymbol{\zeta}}_j\|)^2}{\mathcal{J}_i}+\frac{(\|\tilde{\tilde{\boldsymbol{\zeta}}}_j\|)^2}{\mathcal{J}_j}}, \quad (38)$$

where

$$\widetilde{\mathbf{ss}}'_j=\frac{1}{2}[\|\boldsymbol{\eta}_j\|\mathrm{sgn}(\tilde{u}^{rot}_{\eta j}),\|\boldsymbol{\eta}_j\|\mathrm{sgn}(\tilde{u}^{rot}_{\xi j}),0], \quad (39)$$

$\widetilde{\widetilde{\mathbf{ss}}}'_j=-\widetilde{\mathbf{ss}}'_j$ and

$$\mathbf{A}_j=\frac{1}{m_i}\sum_{l(i)}\mathbf{e}_j\cdot\mathbf{F}_{l(i)}-\frac{1}{m_j}\sum_{l(j)}\mathbf{e}_j\cdot\mathbf{F}_{l(j)}+\frac{1}{\mathcal{J}_i}\sum_{l(i)}(\mathbf{e}_j\cdot\mathbf{M}_{l(i)})\times\tilde{\mathbf{s}}'_j-\frac{1}{\mathcal{J}_j}\sum_{l(j)}(\mathbf{e}_j\cdot\mathbf{M}_{l(j)})\times\tilde{\tilde{\mathbf{s}}}'_j+\boldsymbol{\omega}_i\times\frac{d\tilde{\mathbf{s}}'_j}{d\,t}-\boldsymbol{\omega}_j\times\frac{d\tilde{\tilde{\mathbf{s}}}'_j}{d\,t}. \quad (40)$$

The above expressions are necessary for the definitions of some collisional torques. Therefore we have the collisional torque operating from particle i to particle j as

$$\tilde{\mathbf{M}}^{coll}_j=\begin{cases}0 & \text{for} \quad \|\tilde{\mathbf{u}}'^{\,lin}_{tj}\|=\|\tilde{\mathbf{u}}'^{\,rot}_{tj}\|=0,\\ \tilde{\mathbf{M}}^{rol}_j & \text{for} \quad \|\tilde{\mathbf{u}}'^{\,lin}_{tj}-\tilde{\mathbf{u}}'^{\,rot}_{tj}\|=0,\\ \tilde{\mathbf{M}}^{sli}_j & \text{for} \quad \|\tilde{\mathbf{u}}'^{\,lin}_{tj}-\tilde{\mathbf{u}}'^{\,rot}_{tj}\|>0,\end{cases} \quad (41)$$

where $\tilde{\mathbf{M}}^{sli}_j$ is the coupled torsion-sliding torque, $\tilde{\mathbf{M}}^{rol}_j$ represents the coupled torsion-rolling torque. It should be noted that transition from the local system of coordinates to the global ones reads

$$\tilde{\mathbf{M}}^{sli}_j=\mathbf{e}^T_j\cdot(\tilde{\mathbf{M}}'^{\,sli}_j+\tilde{\mathbf{M}}'^{\,tor}_j),$$

$$\tilde{\mathbf{M}}^{rol}_j=\mathbf{e}^T_j\cdot(\tilde{\mathbf{M}}'^{\,rol}_j+\tilde{\mathbf{M}}'^{\,tor}_j). \quad (42)$$

We define the torsion torque as $\widetilde{\mathbf{M}}'^{\,tor}_j=[0,0,\widetilde{M}^{tor}_{\zeta\,j}]^T$ and according to [33] we obtain

$$\tilde{M}^{tor}_{\zeta j}=-\frac{1}{2}\mathcal{T}(\lambda_j)\|\boldsymbol{\eta}_j\|\mu(\|\tilde{\mathbf{u}}'^{\,lin}_{tj}\|)N_{\zeta\,j}\,\mathrm{sgn}(\omega_{\zeta i}-\omega_{\zeta j}), \quad (43)$$

where the function $\mathcal{T}(\lambda_j)$ reads

$$\mathcal{T}(\lambda_j)=\begin{cases}\dfrac{4}{9}\dfrac{(4-2\lambda_j^2)E(\lambda_j)+(\lambda_j^2-1)K(\lambda_j)}{\pi} & \text{for } \lambda_j\leqslant 1,\\ \dfrac{4}{9}\dfrac{(4-2\lambda_j^2)E\left(\dfrac{1}{\lambda_j}\right)+\left(2\lambda_j^2-5+\dfrac{3}{\lambda_j^2}\right)K\left(\dfrac{1}{\lambda_j}\right)}{\pi\lambda_j} & \text{for } \lambda_j>1\end{cases}. \quad (44)$$

The limiting values of the function $\mathcal{T}(\lambda_j)$ are $\mathcal{T}(0)=\frac{2}{3}$ for torsion without sliding and $\lim_{\lambda_j\to\infty}\mathcal{T}(\lambda_j)=0$ for sliding without torsion. Moreover, we introduce the sliding torque as

$$\widetilde{\mathbf{M}}_j'^{\,sli}=\widetilde{\mathbf{s}}_j'\times\mathbf{T}_j'^{\,sli}. \tag{45}$$

Using an idea included in [34] we determine the rolling torque as

$$\widetilde{\mathbf{M}}_j'^{\,rol}=\widetilde{\mathbf{s}}_j'\times\mathbf{T}_j'^{\,rol}-\widetilde{\mathbf{ss}}_j'\times\mathbf{N}_j', \tag{46}$$

where $-\widetilde{\mathbf{ss}}_j'\times\mathbf{N}_j'$ is the torque created on the penetration width (6). As noted in [34], the torque $-\widetilde{\mathbf{ss}}_j'\times\mathbf{N}_j'$ exists because the contact between two particles is not a single point but, due to deformation of both bodies, is a finite area.

Summarizing this subsection: we determined a full description of the forces and torques occurring in a collision. We neglect here a mathematical description of the collisional force $\mathbf{P}_j^{b\ coll}$ and torque $\widetilde{\mathbf{M}}_j^{b\ coll}$ acting between the particle-wall because one can easily produce these formulas taking into account $\dot{\mathbf{x}}_j=\mathbf{0}$, $\boldsymbol{\omega}_j=\mathbf{0}$, etc., in the above expressions. More details concerning particle-wall interaction can be found in [36].

III. SOLUTION PROCEDURE

Throughout this section we will show how to handle the system of ordinary differential equations (21) and (22) in order to simulate the dynamics of multiparticle collisions. The above system is mathematically complex, and therefore requires a numerical approach. However, estimation of collision duration is needed for numerical stability. Therefore the analytic solution for a simplified two-particle collision requires the calculation of important quantities, i.e., collisional time.

A. Analytic solution for a binary collision

In this subsection we present an analytical solution for the simplified case of a two-particle collision in one dimension. In this case, we use the fractional interaction law of the repulsive force (30). Additionally, we neglect all forces eventually acting on a particle and we assume a central collision. We alos omit angular motion and all friction phenomena occurring between contacting particles. Against this background, let us describe the motion of two colliding particles as

$$m_1\ddot{x}_1=-R(\zeta),$$

$$m_2\ddot{x}_2=R(\zeta), \tag{47}$$

where $\zeta=r_1+r_2-(x_2-x_1)$ and $R(\zeta)$ represents the fractional interaction law (30). It should be noted that the above system of equations is valid for $t\geqslant t^b$, where t^b is the time when the collision starts. According to definition 1 we obtain $\zeta(t^b)=0$. Assuming the conversion degree is positive ($\alpha\geqslant 0$) we derive a simplified form of the repulsive force (30) as

$$R(\zeta)=c^\alpha k^{1-\alpha}\,{}_{t^b}D_{t^e}^{\alpha}(\zeta). \tag{48}$$

Introducing novel variables

$$w=\frac{m_1x_1+m_2x_2}{m_1+m_2},\quad v=x_1-x_2, \tag{49}$$

we transform system (47) to the following form:

$$\ddot{w}=0,$$

$$\ddot{v}=-c^\alpha k^{1-\alpha}\left(\frac{1}{m_1}+\frac{1}{m_2}\right)[{}_{t^b}D_{t^e}^{\alpha}(v)+(r_1+r_2)\,{}_{t^b}D_{t^e}^{\alpha}(1)]. \tag{50}$$

It should be noted that the fractional derivative ${}_{t^b}D_{t^e}^{\alpha}(1)$ calculated from the unit function is not zero.

The above system of differential equations can be solved analytically. Using the Laplace transformation and introducing initial conditions $v(t^b)=r_1+r_2$, $\dot{\zeta}(t^b)=\dot{x}_1(t^b)-\dot{x}_2(t^b)$ we obtain a solution to the system (50) as

$$w(t)=\frac{m_1\dot{x}_1(t^b)+m_2\dot{x}_2(t^b)}{m_1+m_2}(t-t^b)+\frac{m_1x_1(t^b)+m_2x_2(t^b)}{m_1+m_2},$$

$$\zeta(t)=v(t)+r_1+r_2=[\dot{x}_1(t^b)-\dot{x}_2(t^b)](t-t^b)\times E_{2-\alpha,2}(-A(t-t^b)^{2-\alpha}), \tag{51}$$

where

$$A=c^\alpha k^{1-\alpha}\left(\frac{1}{m_1}+\frac{1}{m_2}\right) \tag{52}$$

and $E_{2-\alpha,2}$ is the Mittag-Leffler function. According to [22] this function is defined as

$$E_{\delta,\nu}(t)=\sum_{l=0}^{\infty}\frac{t^l}{\Gamma(\delta l+\nu)}. \tag{53}$$

In formula (51) $w(t)$ represents the motion of the particles' centers of mass and $\zeta(t)$ denotes the overlap (5). Differentiating $\zeta(t)$ over time we find a normal component of the relative velocity of colliding particles as follows

$$\dot{\zeta}(t)=[\dot{x}_1(t^b)-\dot{x}_2(t^b)][E_{2-\alpha,2}(-A(t-t^b)^{2-\alpha})-A(2-\alpha)(t-t^b)^{2-\alpha}E_{2-\alpha,2}^{(1)}(-A(t-t^b)^{2-\alpha})], \tag{54}$$

where $E_{\delta,\nu}^{(1)}(t)$ is the first derivative of the Mittag-Leffler function, which can be calculated as

$$E_{\delta,\nu}^{(1)}(t)=\frac{d}{dt}[E_{\delta,\mu}(t)]=\sum_{l=1}^{\infty}\frac{lt^{l-1}}{\Gamma(\delta l+\nu)}. \tag{55}$$

To calculate the algebraic form of the repulsive force we need to put $\zeta(t)$, which is included in expression (51), into formula (48). According to fractional calculus [22,23,35] we apply Leibniz rule and we obtain the repulsive force as

$$R(\zeta(t)) = c^{\alpha}k^{1-\alpha}[\dot{x}_1(t^b) - \dot{x}_2(t^b)]\sum_{l=0}^{\infty}\left\{\frac{\Gamma(\alpha+1)}{\Gamma(\alpha-l+1)\Gamma(l+1)\Gamma(l-\alpha+2)} \times (t-t^b)^{l-\alpha+1}E^{(l)}_{2-\alpha,2}(-A(t-t^b)^{2-\alpha})\right\}, \quad (56)$$

where $E^{(l)}_{2-\alpha,2}(-A(t-t^b)^{2-\alpha})$ represents the derivative of the Mittag-Leffler function of order l. The limiting value of the function $R(\zeta(t))$ is $\lim_{t\to t^e}R(\zeta(t))=0$. This limit determines the collisional time of two contacting particles as $t^{coll}=t^e-t^b$. An explicit solution of formula (56) in order to find t^{coll} is impossible. Therefore we use some approximation to estimate the collisional time by the following expression

$$t^{coll} \geqslant \left((1.64)^{1-\alpha}\frac{\Gamma(4-\alpha)}{A}\right)^{1/(2-\alpha)}, \quad (57)$$

where A is predicted by formula (52). Expression (57) is suitable for rough estimation of the time increment Δt^{coll} used in numerical calculations.

Extending our considerations concerning the behavior of formula (57) we found that for $\alpha=0$ this formula reduces to $t^{coll}\geqslant\sqrt{9.84/A}$. This expression agrees well with the collisional time calculated by the linear interaction law [13], where the damping coefficient is assumed to be zero.

B. Numerical solution

An accurate solution to this problem was obtained by integrating the system of ordinary differential equations (21) for particles moving individually using Numerical Recipe routines [37]. Tracing the motion of individual particles over time we need to detect particle collisions in order to take into account collisional forces and torques in the system of differential equations. Using results presented in [25–27] we have chosen the linked cell method to detect a collision.

It should be noted that during particle collisions we need to solve system (22), where the fractional interaction law (30) occurs. In this case we have a system of ordinary differential equations with a mixture of operators: the integer derivative of maximal order equals two, the fractional integral of order $-\alpha_j$ and the fractional derivative of order α_j. Using fractional calculus [22,23,35] we present discrete forms of the fractional operators which are suitable in our algorithm. Let us consider the duration of a collision over time $t\in\langle t^b,t^e\rangle$ where t^b represents the time when the collision starts and t^e is the time when the collision ends. We introduce the division ΔN of the collisional time $t^{coll}=t^e-t^b$ into several time steps. Thus we obtain

$$\Delta t^{coll} = \frac{t^{coll}}{\Delta N} \quad (58)$$

and $t_l=t^b+l\Delta t^{coll}$, for $l=0,\ldots,\Delta N$. If a function $f(t)$ is constant within the step Δt^{coll} then the discrete form of the Caputo fractional derivative (32) becomes

$${}^{C}_{t^b}D^{\alpha}_{t^e}f(t) = \frac{1}{\Gamma(n-\alpha+1)}\left[A_1(t^e-t^b)^{n-\alpha} + \sum_{l=2}^{\Delta N}(A_l-A_{l-1})(t^e-t_{l-1})^{n-\alpha}\right], \quad (59)$$

where $\alpha\in\mathcal{R}^+$, $n=[\alpha]+1$ and $[\cdot]$ denotes an integer part of a real number, $A_l=f^{(n)}(t_l)$ where $f^{(n)}$ is the derivative of integer order n. Note that in formula (59) $f(t)$ denotes the overlap (5). Taking the above assumptions into account we obtain the discrete form of the Riemann-Liouville fractional integral (33) as

$${}_{t^b}I^{\beta}_{t^e}f(t) = \frac{1}{\Gamma(\beta+1)}\left[B_1(t^e-t^b)^{\beta} + \sum_{l=2}^{\Delta N}(B_l-B_{l-1})(t^e-t_{l-1})^{\beta}\right], \quad (60)$$

where $\beta\in\mathcal{R}^+$ and $B_l=f(t_l)$. The discrete forms of the fractional operators make it possibile to integrate system (22) using any predictor-corrector procedure [37] with correction of the time step Δt^{coll}. The correction of the time step provides measures that allow us to determine the begin time, when particles enter into a collision, and the end time of particle collisions. It should be noted that the begin and end times are determined by several definitions presented in the previous section. Using fractional calculus [22] we found that the accuracy of the discrete form of the fractional derivative (59) is equaled to $O((\Delta N)^{-4})$.

We perform a numerical test in order to find the appropriate value of ΔN. This test concerns the impact of a steel particle onto a bottom plate. Figure 2 shows the influence of the division number ΔN on the behavior over time of the overlap (5), the relative velocity (14) and the repulsive force (30). The analytic solution which we presented in the previous subsection is included in the figure. In the figure $r=3\times10^{-3}$ m, $\varrho=7680$ kg/m^3, $k=4615380$ kg/s^2, $c=128.1$ kg/s, $\alpha=0.2$ and the initial (impact) particle velocity is set at $\dot{\zeta}(0)=1$ m/s. In this case we obtained a value of the collisional time as $t^{coll}=38.6\times10^{-6}$ s. Using formula (57) we estimated $\tilde{t}^{coll}$ to be $\tilde{t}^{coll}=37.8\times10^{-6}$ s. This underestimation of the collisional time ($\tilde{t}^{coll}<t^{coll}$) issues from the linear approximation of the solution to equation $R(\zeta(t))=0$, where $R(\zeta(t))$ is represented by formula (56). Extending our considerations we can observe plausible agreement between the numerical data obtained for different ΔN and the analytic solution. Nevertheless we should analyze what happens to the overlap, the relative velocity and the repulsive force at the time when the collision ends. Table I shows the quantities which are dependent on the division ΔN for the assumed value of the collisional time at $t^{coll}=38.6\times10^{-6}$ s. Direct

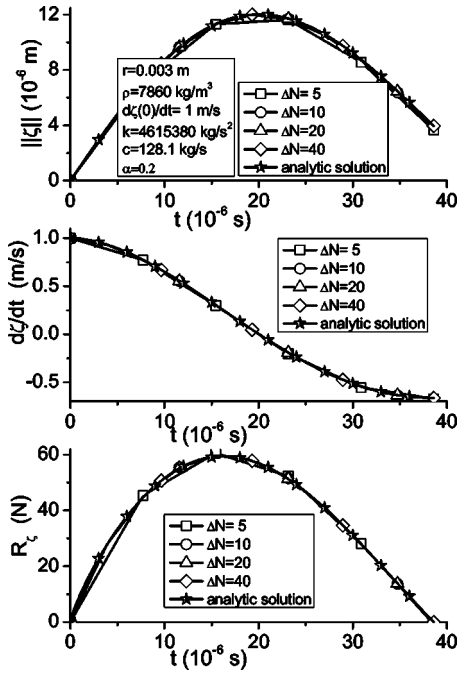

FIG. 2. Behavior of the overlap (top), relative velocity (middle), and force (bottom) over time for different lengths of the time step Δt^{coll}.

comparison of the numerical results with the analytic solution shows that $\Delta N=5$ does not present satisfactory results. However, we can observe that within the range from $\Delta N=20$ to $\Delta N=40$ the repulsive force is close to zero and the other numerical quantities (the overlap and the relative velocity) agree well with the analytic solution. Based on the above results, $\Delta N=30$ was chosen order to keep good agreement with the analytic solution.

Next, taking formulas (27) and (41) into account in calculations of particle contacts, we need to find an accurate time needed to detect the switching between torsion-sliding, sliding and rolling processes. A simple way to calculate the switching time is to use a linear approximation method, as described in the paper [34].

Next we consider a problem occurring in the calculations of friction forces (34) and (38) and the torsional torque (43). When the relative velocity at the contact point changes from negative to positive or vice versa, it indicates that the signum function $\mathrm{sgn}(x)$ changes sign very fast in the above expressions. This is not desirable as it influences the stability and convergence of the numerical calculations in a significant way. Therefore we modified the signum function introducing

$$\widetilde{\mathrm{sgn}}(x)=\begin{cases}-1 & \text{for } x\leqslant-\epsilon_2,\\ \dfrac{1}{\epsilon_2-\epsilon_1}x+\dfrac{\epsilon_1}{\epsilon_2-\epsilon_1} & \text{for } -\epsilon_2\leqslant x\leqslant-\epsilon_1,\\ 0 & \text{for } -\epsilon_1\leqslant x\leqslant\epsilon_1,\\ \dfrac{1}{\epsilon_2-\epsilon_1}x-\dfrac{\epsilon_1}{\epsilon_2-\epsilon_1} & \text{for } \epsilon_1\leqslant x\leqslant\epsilon_2,\\ 1 & \text{for } x\geqslant\epsilon_2,\end{cases} \tag{61}$$

where x is the actual value registered during a contact (the relative velocity), ϵ_1, ϵ_2 are numerical coefficients. This function is robust for $x\to 0$ and gives a satisfactory result.

IV. RESULTS AND THEIR ANALYSIS

To illustrate the benefits of the fractional interaction law (30) in the dynamics of arbitrary multiparticle collisions, we will first demonstrate how this law operates in simple cases connected with a one dimensional problem. First, we simulate a central collision between two particles. Figure 3 shows the dynamics of a two-particle collision, which is represented by some variations in the overlap $\|\zeta\|$ (5), the linear relative velocity $\dot{\zeta}=u_\zeta^{lin}$ (14) and the repulsive force R_ζ (30) over time for different levels of the conversion degree α. Here we neglect the index j because only two particles collide. Moreover, all vectors are converted to scalar values when a one dimensional problem is considered. In Fig. 3 $m_{eff}=m_1m_2/(m_1+m_2)=7.06858\times10^{-6}$ kg, $r_1=r_2=3\times10^{-3}$ m, $k=5000$ kg/s^2, $c=0.1$ kg/s. The initial relative velocity is set at $\dot{\zeta}=0.5$ m/s and three groups of variations in the conversion degree are taken into account. The first group is for $\alpha<0$ (left column), the second is for $0\leqslant\alpha\leqslant1$ (middle column) and the third represents $\alpha>1$ (right column). Within the range $0\leqslant\alpha\leqslant1$ we observe that collisional time t^{coll} increases when α is increased. It should be noted that the collisional time is registered when the repulsive force R_ζ reaches zero, as presented in several definitions in the previous sections. Therefore, the overlap $\|\zeta\|$ has some values at the time when a collision ends and deformations of the particles' surfaces are noted. Analyzing the behavior of the relative velocity $\dot{\zeta}$ over time we notice that this velocity changes direction for small values of α, which means that particle rebounds dominate. When α increases we can see that the relative velocity tends to zero, which means that particles stick together. In other words, if $\alpha=0$, no viscous term in Eq. (30) may occur and all the impact energy must be due to

TABLE I. Influence of the division number ΔN of the collisional time t^{coll} on the overlap, the relative velocity, and the repulsive force for $t=t^e$.

	$\Delta N=5$	$\Delta N=20$	$\Delta N=40$	Analytic
Δt^{coll} (10^{-7} s)	77.20	19.30	9.65	$\to0$
$\|\zeta\|$ (10^{-6} m)	3.65856	3.94248	3.94429	3.94422
$\dot{\zeta}$ (m/s)	−0.67213	−0.66377	−0.66317	−0.63317
R_ζ (N)	−0.84688	−0.01383	−0.00006	0

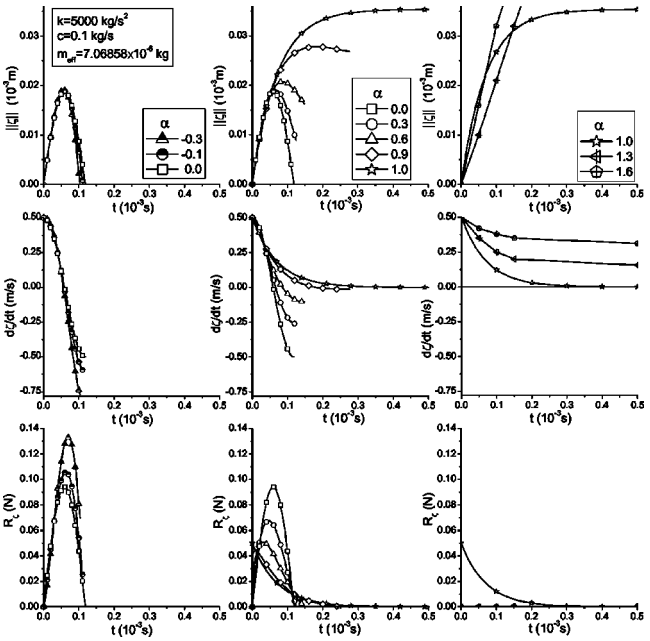

FIG. 3. Behavior of the overlap (top), relative velocity (middle), and force (bottom) over time for the fractional interaction law.

elasticity. In this case the overlap reaches zero at the same time as the repulsive force reaches zero. If $\alpha=1$, on the other hand, the impact energy is transfered through the viscous term.

Extending our considerations for $\alpha>1$ we observe (right column on Fig. 3) that the repulsive force is not generated and tends to zero for $t^{coll}\rightarrow\infty$, and therefore the overlap increases to high and unrealistic values. Moreover, the relative velocity does not change direction and particles undergo the next time steps of the calculations. According to definition 7, presented in the previous section, the fragmentation of particles or permanent cohesion of particles is a direct result of the plastic flow of their contacting surfaces. The contacting surfaces are destroyed because deformations of contacting particles become sufficiently large so as to exceed the elastic limit of the materials, and we noticed particle clusterisations. This process is observed experimentally in [30,32] and may be modeled by the fractional interaction law (30).

Next we considered the behavior of the overlap, relative velocity and repulsive force for $\alpha<0$ (left column on Fig. 3). Larger negative values of the conversion degree α decrease the collisional time. The relative velocity changes direction but at the end time reaches larger absolute values in comparison to the initial relative velocity. As this is unrealistic all the solutions for $\alpha<0$ are not taken into account. The aim of this example is to show the power of fractional calculus, where more solutions are obtained in comparison to classical differential and integral operators having integer order. However, we need to choose which solutions obtained by fractional calculus are suitable physically.

In Fig. 3 we constructed several mappings for the relative velocity-overlap (left), force-overlap (middle) and force-relative velocity (right) where α changes from negative to positive values. Analyzing these mappings we found a set of criteria necessary to predict different states of particle collisions included in the definitions in the previous section. It should be noted that small positive values of α predict particle rebounds when particle deformations are practically negligible. When α tends to unity we also observe particle rebounds but particle deformations are visible and more energy is dissipated. As indicated in the left chart in Fig. 3, when α is above unity the repulsive force is not generated and this indicates instability in particle collisions. This instability takes the form of particle fragmentation or permanent clusterization of particles after the collision. Therefore the conversion degree α is a ratio of the impact energy over the specific energy needed for the destruction of particle surfaces. This assumption should be validated experimentally, and this is the aim of our future investigations. It should be noted that when the physical properties of colliding granular materials and the impact energy are fixed we still observe different values of energy dissipation after the collision. This can be easily seen when we compare the particle collisions for particles with smooth surfaces and for rough ones. The fractional interaction law can simulate this because the conversion degree α can change. (See Fig. 4.)

In order to compare the fractional interaction law with other interaction laws, changes over time of the overlap, the relative velocity and the repulsive force for two-particle collision were presented. We assumed the parameters of colliding particles to be $r_1=r_2=3\times10^{-3}$ m, $m_{eff}=7.06858\times10^{-6}$ kg, $\dot{\zeta}=0.5$ m/s. Moreover, we assumed the collision time between two colliding bodies the $t^{coll}=10^{-4}$ s and the restitution coefficient $e_r=0.5$. These assumptions are necessary to calculate the set of coefficients required by different interaction laws, depending on the type of interaction law chosen. In Table II we list all the coefficients. Some of the expressions applied to calculate the coefficients for linear [13] and hysteretic [15] laws can be found in [19]. The formulas of the coefficients used in the linear interaction law assumed that at the end time of a collision the overlap is zero. In Table II the "linear1" represents the above case. We assumed that the repulsive force reaches zero at the end time

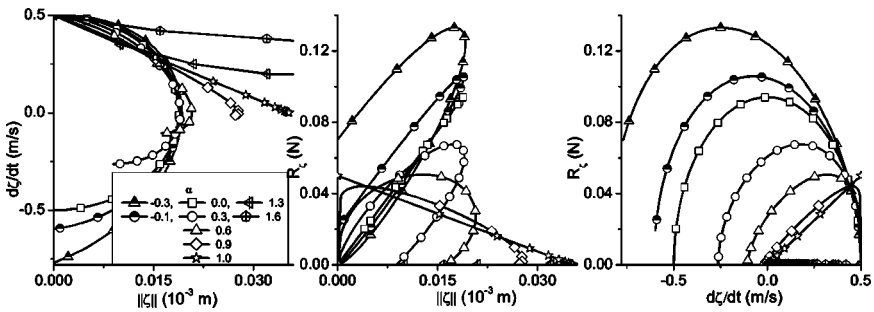

FIG. 4. Mapping the relative velocity-overlap (left), force-overlap (middle), and force-relative velocity (right) for the fractional interaction law.

TABLE II. Coefficients for colliding particle surfaces being dependent on the interaction law used.

Law	Coefficients
linear1	$k_n=7316$ kg/s^2, $c_n=0.0979$ kg/s
linear2	$k_n=5225$ kg/s^2, $c_n=0.0981$ kg/s
nonlinear	$\tilde{k}=1392000$ kg/s$^2\sqrt{\text{m}}$, $\tilde{c}=33.885$ kg/s$\sqrt{\text{m}}$
hysteretic	$k_1=3924$ kg/s^2, $k_2=15697$ kg/s^2
fractional	$k=5225$ kg/s^2, $c=0.297$ kg/s, $\alpha=0.3197$

of a collision. Thus we have a set of coefficients called "linear2" also used for the linear interaction law. For the nonlinear [14] and fractional laws we performed a numerical test to find the values of the coefficients which allow us to keep the assumed collision time and the restitution coefficient in a two-particle contact. It should be noted that we obtained many sets of coefficients for the fractional interaction law. Therefore, for this law, we establish the spring coefficient, which has the same value as for the linear interaction law. Figure 5 shows the behavior of the overlap (top chart), the relative velocity (middle chart) and the repulsive force (bottom chart) over time where different interaction laws are taken into account. Analyzing this figure we can confirmed that the interaction law fulfilled our assumptions concerning the collisional time and the restitution coefficient. It should be noted that the repulsive force changes direction in the linear interaction law (linear1) for the set of coefficients calculated under the formulas found in [19]. This shows a deficiency in numerical calculations and should be rejected. Some changes in the values of the above coefficients give satisfactory results in the linear interaction law (linear2). However, the repulsive force in the linear interaction law has a value at the beginning time which is independent on the set of coefficients used. This is also unrealistic behaviour under the linear interaction law.

Using different interaction laws we observed different overlaps at the end time of a collision. The greatest overlap is for the hysteretic law and decreases for the fractional in through the nonlinear to the linear one. Note that we can find another set of coefficients for the fractional law that fulfill our assumptions and allows us to obtain another value of the overlap at the end time of collision.

When we have determined all the parameters necessary to describe the dynamics of particle impacts we then obtain some values of the collisional time and the restitution coefficient for this case. However, if we still keep the above parameters but increase or decrease the surface roughness of the colliding particles then we obtain values of the collisional time and the restitution coefficient which differ in comparison to the previous values. As we did not change the physical properties of this granular material, we have to maintain the steady value of the spring coefficient in all the interaction laws. Changing only the damping coefficient in the linear and nonlinear laws and the unloading slope k_2 in the hysteretic law does not guarantee that we will obtain accurate values of the collisional time and the restitution coefficient reflecting the above cases. This is a disadvantage of the well-known interaction laws. In the fractional interaction law we

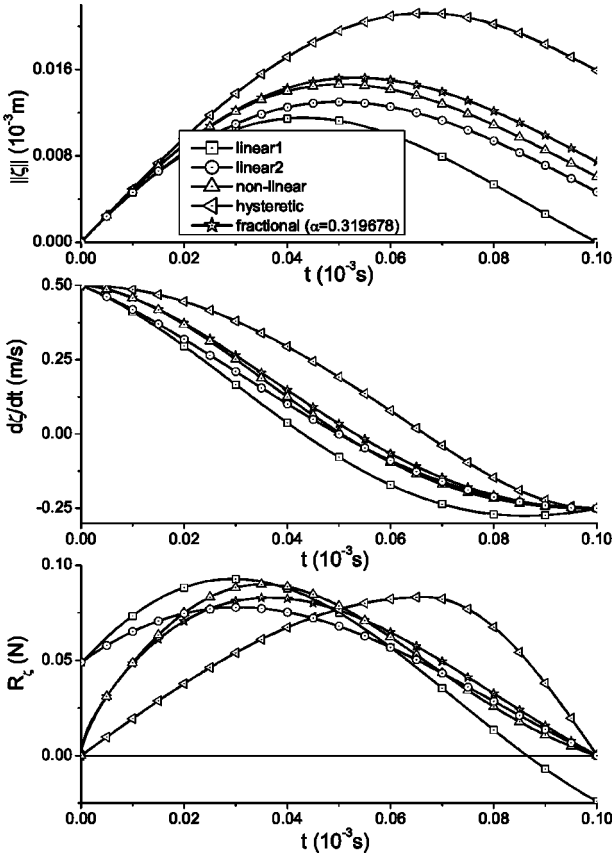

FIG. 5. Comparison of the overlap (top), relative velocity (middle), and force (bottom) over time for different interaction laws.

have an additional parameter called the conversion degree α which causes some changes in the collisional time and the restitution coefficient. However, this requires some experimental data involving the impact dynamics of smooth and rough particles. These data will provide measures that allow some links to be made between the experiment and the coefficients of the fractional law.

In order to verify the validity of the interaction laws for multiparticle collisions, the energies dissipated at each contact were compared. Here we introduce a measure of energy dissipation during multiparticle collisions which is the ratio of the kinetic energy evaluated in time over the initial kinetic energy. We define the total ratio of energy lost through multiparticle collisions as where the superscript 0 refers to the initial kinetic energy examined at time $t=0$ *s* and *nc* is the total number of colliding particles.

We used a set of particles *np* vertically stacked over a bottom plate as shown in [18,19]:

$$\varepsilon = 1 - \frac{\sum_{i=1}^{nc} m_i \dot{x}_i^2}{\sum_{i=1}^{nc} m_i^0 (\dot{x}_i^0)^2}. \tag{62}$$

We assumed the following conditions $r_i=0.0015$ m, $m_i=1.41\times10^{-5}$ kg, $\dot{x}_i=-0.5$ m/s, for $i=1,\ldots,np$. Gravity is

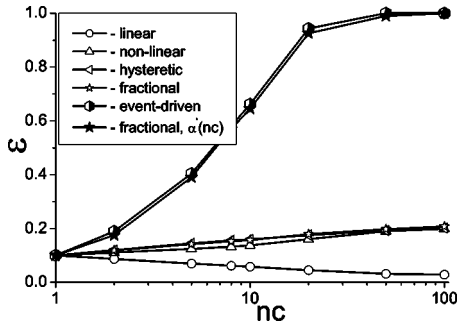

FIG. 6. Energy dissipation during multiparticle collisions for different interaction laws.

set at zero. Taking into account the results presented by [18] we calculated the energy dissipation as a function of the number of considered particles *np*, which becomes the number of colliding particles *nc* when at the begin time of the collision the distances between spheres equal zero $l_j^0=0m$, for $j=1,\ldots,nc$. Note that $j=1$ represents a collision between the first particle and the bottom plate and $j=nc$ is a collision between the topmost particles. We also assume the collisional time between two colliding bodies $t^{coll}=10^{-4}$ s and the restitution coefficient $e_r=0.945$. These assumptions are necessary to calculate some coefficients depending on the type of interaction law chosen. The coefficients represent a collision between two particles or between a particle and the bottom plate, where the plate mass is infinite.

Figure 6 shows the energy dissipation as being dependent on the number of collisions *nc* for different interaction laws used in the molecular dynamics method and also in the event driven method [20,25]. For linear, nonlinear and hysteretic laws we noted the same dependencies as in [18,19]. This means that the "detachment" effect occurs. First, we considered the fractional interaction law for a steady value of the conversion degree $\alpha_j=0.0258$, for all binary collisions. In this case we obtained similar results for the hysteretic and fractional interaction laws. Thus the "detachment" effect also occurs in the fractional interaction law for the steady value of α_j. As written in [18] the kinetic energy obtained from the event driven technique is dissipated totally for $nc\cdot(1-e_r)$ large. It should be noted that the basic interaction laws are valid for two-particle collisions which are completely independent of other collisions. However, in multiparticle collisions, we need to include mutual dependencies between several binary collisions. Taking this fact into account, we can obtain satisfactory results when the conversion degree α_j changes in relation to the number of colliding particles. This was explained more precisely in [21]. Therefore we propose $\alpha'(nc)\sim 1+\exp(-nc)$ in order to keep a qualitative agreement with the event driven method. It should be noted that we cannot estimate correctly $\alpha'(nc)$ by direct comparison with the event driven technique. We require experimental data involving multiparticle collisions. This data will provide measures that allow some links to be made between several coefficients in the fractional interaction law and the experiment.

The last example simulates the dynamics of five particles in three dimensional space for two values of the parameter α.

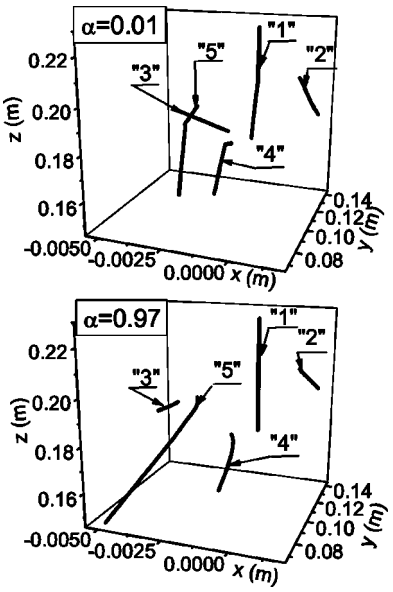

FIG. 7. Behavior of particle trajectories depending on strong ($\alpha=0.01$) and weak ($\alpha=0.97$) repulsions.

The first value $\alpha=0.01$ indicates the strong repulsive state, i.e., particles rebound almost without dissipation of their energy. The second one for $\alpha=0.97$ represents the weak repulsive state where most of the impact energy is converted into material viscoelastcity. We can easily observe such states in the real behavior of granular materials, when we consider the collisions for contacting particles with smooth surfaces and for rough ones. For this simulation we assumed the following conditions $r_1=0.02$ m, $r_2=0.01$ m, $r_3=0.007$ m, $r_4=0.005$ m, $r_5=0.009$ m, $\varrho_1=\varrho_4=2000$ kg/m^3, $\varrho_2=\varrho_3=\varrho_5=1000$ kg/m^3, $\mathbf{x}_1=[0.0,0.1,0.23]$ m, $\mathbf{x}_2=[0.001,0.125,0.205]$ m, $\mathbf{x}_3=[-0.002,0.090,0.198]$ m, $\mathbf{x}_4=[-0.004,0.120,0.186]$ m, and $\mathbf{x}_5=[-0.001,0.1,0.18]$ m. Moreover, we consider a situation where a particle with an initial linear velocity $\mathbf{u}_1=[0,0,-5]$ m/s collides at different moments in time with particles which initially do not move ($\mathbf{u}_j=[0,0,0]$ m/s, for $j=2,\ldots,4$). Particles do not rotate initially ($\boldsymbol{\omega}_i=\mathbf{0}$ 1/s), gravity is set to zero and $k=1000$ kg/s^2, $c=1$ kg/s for each pair of colliding particles. We also simplified values of the friction coeffcients putting into Eq. (35) $a=0$ and $\mu_s=0.5$ for each pair of colliding particles. Figure 7 shows the trajectories of the mass centers of five particles in three dimensional space for strong and weak repulsions as a reaction to the impact dynamics. The particles are numbered from 1 to 5. This simulation does not reflect the real motion of particles because we neglect external forces, i.e., the gravitational force. We can only show how the fractional interaction law operates in the above conditions as being dependent on the conversion degree α. In the strong repulsive state ($\alpha=0.01$) we observe linear particle trajectories. As α is increased and reaches the weak repulsive state ($\alpha=0.97$) we noticed different particle trajectories in comparison to the previous state. According to the results presented in Fig. 3 we can say that duration over time of the repulsive force, which is longer over time for higher values of α, has a significant influence on the particle trajectories.

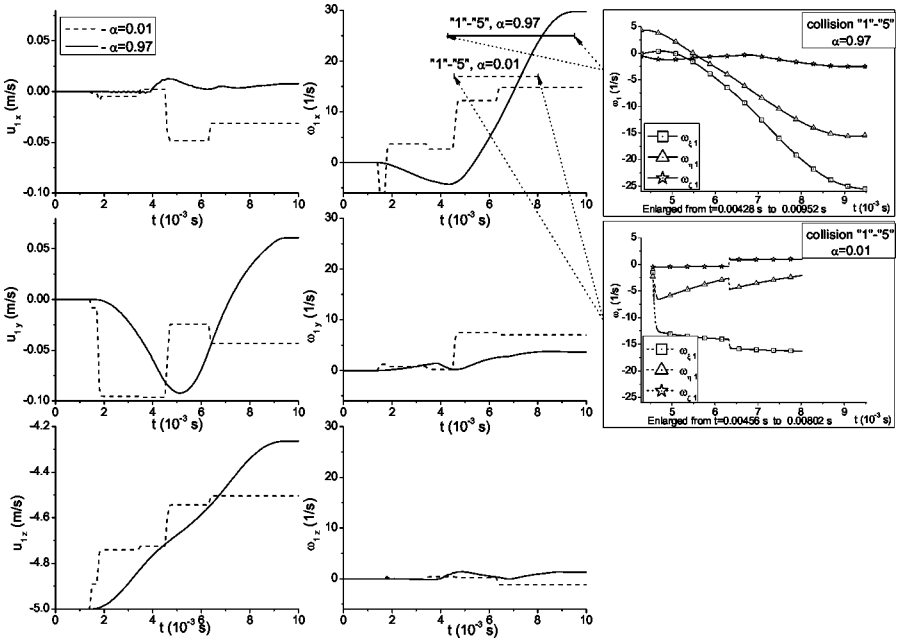

FIG. 8. Linear and angular velocities of particle 1 over time for strong ($\alpha=0.01$) and weak ($\alpha=0.97$) repulsions.

In order to explain more precisely what happens to particle trajectories in strong and weak repulsive states, the velocities of one individual particle were analyzed. Figure 8 shows the linear and angular velocities of particle 1 over time in the global system of coordinates (x,y,z). In this figure the dashed lines represent particle velocities in the strong repulsive state, whereas continous lines indicate the weak repulsive state. We can observe clear jumps in particle velocities over time for the strong repulsive state. This is a result of the duration of a collision determined by the collisonal time between a pair of contacting particles. In this state we can notice binary collisions because several collisional times between the different pairs of contacting particles have shorter values in comparison to their separation times, where particles move individually. However, in the weak repulsive state we observe continous changes in particle velocities without the distinction of any jumps. This means that several collisional times between the pairs of contacting particles overlap each other. So binary collisions are not distinguished here.

Moreover, we analyzed, in the local system of coordinates (ξ,η,ζ), the angular velocities over time of particle 1, which collides with particle 5. In the strong repulsive state we observe smaller values of ω_ξ and ω_η (these velocities are angular velocities predicted in the tangent plane as shown in Fig. 1) in comparison to the weak repulsive state. This means that torsion-sliding friction dominates in the strong repulsive state, where binary collisions are noted. In the weak repulsive state we observe that the angular velocities ω_ξ and ω_η have higher values than in the strong repulsive state. Thus we expect the torsion-rolling friction between particles 1 and 5. However, multiparticle collisions are noted in the weak repulsive state.

In order to prove where binary or multiparticle collisions occur, some distributions of collisional times over the duration time of calculations are presented. Figure 9 presents the sequence of segments of collisional times over the time of observation for strong and weak repulsive states. Continous segments represent collisional times for weak repulsion whereas strong repulsion is denoted by the dashed segments. Each segment representes one binary collision between a pair of contacting particles, i.e., 1-3 means the collision between particle 1 and particle 3. Analyzing this figure we observe longer collisional times for the weak repulsive state in comparison to the collisonal times for the strong repulsive state. Moreover, the collisional times ovelap in the weak repulsive state, therefore multiparticle collisions occur.

V. CONCLUDING REMARKS

We used the molecular dynamics method to model the motion of individual spherical particles in three-dimensional space. We introduced a novel mathematical description of this method which takes into account the division of the collision process into an impact phase, contact phase and another phase formed after the contact phase. We assumed that the impact phase and the phase formed after the contact phase are infinitesimally short in time. We redefined the collisional time so that it is predicted by the repulsive force-

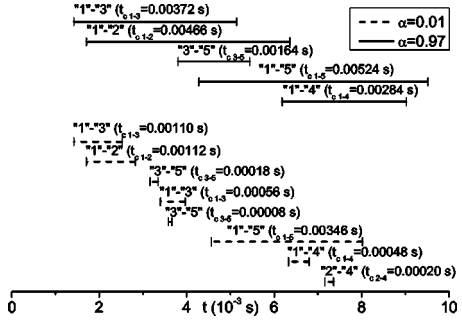

FIG. 9. Sequence of collisional times depending on strong ($\alpha=0.01$) and weak ($\alpha=0.97$) repulsions.

overlap path. On the base of preliminary results [21] we proposed an expression for the repulsive force formulated under fractional calculus. The force can control the energy dissipation and the collisional time for an individual particle colliding with many other particles. In multiparticle collisions, we included the friction mechanism needed for the transition from coupled torsion-sliding friction through rolling friction to static friction. Therefore our model includes multiparticle collisions in arbitrary forms. Using the fractional interaction law one can determine different states of particle repulsions, i.e., strong and weak repulsive states. In the strong repulsive state binary collisions dominate, and torsion-sliding friction is the main friction mechanism. However, within multiparticle collisions rolling friction is observed to be much stronger.

The presented numerical results can be used to realistically model the impact dynamics of an individual particle in a group of colliding particles. In order to tune the model's coefficients we require experimental data involving multiparticle collisions. This data provides measures that allow some links to be made between several coefficients in the fractional interaction law and the experiment.

ACKNOWLEDGMENT

This work was supported by the State Committee for Scientific Research (KBN) under Grant No. 4 T10B 049 25.

[1] J. Geng, E. Longhi, R. P. Behringer, and D. W. Howell, Phys. Rev. E **64**, 060301 (2001).
[2] T. Gregor, U. Tüzün, and D. M. Heyes, Powder Technol. **133**, 203 (2003).
[3] J. P. K. Seville, C. D. Willett, and P. C. Knight, Powder Technol. **113**, 261 (2000).
[4] Z. Zhang and M. Ghadiri, Chem. Eng. Sci. **57**, 3671 (2002).
[5] R. W. Lyczkowski and J. X. Bouillard, Powder Technol. **125**, 217 (2002).
[6] O. Lecoq *et al.*, Powder Technol. **133**, 113 (2003).
[7] B. Painter and R. P. Behringer, Phys. Rev. E **62**, 2380 (2000).
[8] E. Clément *et al.*, Int. J. Mod. Phys. B **7**, 1807 (1993).
[9] F. Rioual, A. Valance, and D. Bideau, Phys. Rev. E **62**, 2450 (2000).
[10] D. Gidaspow, *Multiphase Flow and Fluidization. Continuum and Kinetic Theory Descriptions* (Academic, San Diego, 1994).
[11] G. Balzer, Powder Technol. **113**, 299 (2000).
[12] D. C. Rapaport, *The Art of Molecular Dynamics Simulation* (Cambridge University Press, Cambridge, England, 1995).
[13] P. A. Cundall and O. D. L. Strack, Geotechnique **29**, 47 (1979).
[14] G. Kuwabara and K. Kono, Jpn. J. Appl. Phys., Part 1 **26**, 1230 (1987).
[15] O. R. Walton and R. L. Braun, J. Rheol. **30**, 949 (1986).
[16] B. D. Lubachevsky, J. Comput. Phys. **94**, 255 (1991).
[17] S. Luding *et al.*, Phys. Rev. E **49**, 1634 (1994).
[18] S. Luding *et al.*, Phys. Rev. E **50**, 4113 (1994).
[19] L. Pournin, Th. M. Liebling, and A. Mocellin, Phys. Rev. E **65**, 011302 (2001).
[20] S. McNamara and W. R. Young, Phys. Fluids A **4**, 496 (1992).
[21] J. S. Leszczynski, Granular Matter **5**, 91 (2003).
[22] K. B. Oldham and J. Spanier, *The Fractional Calculus. Theory and Applications of Differentiation and Integration to Arbitrary Order* (Academic, New York, 1974).
[23] I. M. Sokolov, J. Klafter, and A. Blumen, Phys. Today **55**(11), 48 (2002).
[24] H. G. Matuttis, S. Luding, and H. J. Herrmann, Powder Technol. **109**, 278 (2000).
[25] M. P. Allen and D. J. Tildesley, *Computer Simulation of Liquids* (Oxford University Press, Oxford, 1987).
[26] T. Iwai, C. W. Hong, and P. Greil, Int. J. Mod. Phys. C **10**, 823 (1999).
[27] A. Schinner, Granular Matter **2**, 35 (1999).
[28] H. J. Herrmann, J. Phys. A **191**, 263 (1992).
[29] D. Zhang and W. J. Whiten, Powder Technol. **88**, 59 (1996).
[30] H. Krupp, Adv. Colloid Interface Sci. **1**, 111 (1967).
[31] D. Maugis and H. M. Pollock, Acta Metall. **32**, 1323 (1984).
[32] D. S. Rimai, L. P. DeMejo, and R. C. Bowen, in *Fundamentals of Adhesion and Interfaces, 1995*, edited by D. S. Rimai, L. P. DeMejo, and K. L. Mittal (VSP BV Utrecht, Netherlands, 1995), p. 1.
[33] Z. Farkas, G. Bartels, T. Unger, and D. E. Wolf, Phys. Rev. Lett. **90**, 248302 (2003).
[34] D. Zhang and W. J. Whiten, Powder Technol. **102**, 235 (1999).
[35] S. G. Samko, A. A. Kilbas, and O. I. Marichev, *Fractional Integrals and Derivatives. Theory and Applications* (Gordon and Breach, Amsterdam, 1993).
[36] L. Kondic, Phys. Rev. E **60**, 751 (1999).
[37] W. H. Press, S. A. Teukolsky, W. T. Vetterling, and B. P. Flannery, *Numerical Recipes in Fortran90: The Art of Parallel Scientific Computing* (Cambridge University Press, Cambridge, England, 1996).